International Journal of Aerospace and Lightweight Structures
Vol. 3, No. 1 (2013) 109–133

DOI: 10.3850/S201042862013000550

A DESIGN GUIDE OF DOUBLE-LAYER CELLULAR CLADDINGS FOR BLAST ALLEVIATION

Shenfei Liao[a], Zhijun Zheng[b], Jilin Yu[c], and Zhibin Li[d]

CAS Key Laboratory of Mechanical Behavior and Design of Materials, University of Science and Technology of China, Hefei, Anhui 230026, PR China
[a] *liao1985@mail.ustc.edu.cn*
[b] *Corresponding author. zjzheng@ustc.edu.cn*
[c] *jlyu@ustc.edu.cn*
[d] *lizhibin@mail.ustc.edu.cn*

This paper presents a method for the design of a double-layer cellular cladding (DLCC) serving as a protective function against blast load. Two configurations of DLCCs are considered, i.e. cladding with cellular cores of identical density (Cladding-1) and cladding with a higher density cellular core layer close to the blast load (Cladding-2). Shock wave propagations in the two DLCCs are investigated by using a one-dimensional shock model. Single shock front propagates in Cladding-1, while double shock fronts propagate in Cladding-2. A closed-form solution of the critical thickness, which is the minimum thickness required to fully absorb blast load, is given for Cladding-1. Response features of Cladding-2 are analyzed and then the critical thickness of Cladding-2 is determined by optimizing the layer thicknesses. It is demonstrated that, with equal mass of the cover plates, a SLCC is always more efficient than Cladding-1, while Cladding-2 can be more efficient than a SLCC. A design method for Cladding-2 against blast load is further presented. Comparison between the cell-based FE results and the analytical predictions is generally good. The difference in the comparison is analyzed through distribution of strain of Cladding-2 measured by the strain field calculation method.

Keywords: Blast alleviation, Double-layer cellular cladding, Shock wave propagation, Strain distribution, Voronoi honeycomb.

1. Introduction

Cellular materials have superior energy absorption capability and are widely used as the core material of sandwich structures designed as protective structures for blast alleviation [Guruprasad and Mukherjee, 2000a, b; Karagiozova *et al.*, 2010; Lim *et al.*, 2013; Nurick *et al.*, 2009; Theobald *et al.*, 2010]. Sacrificial claddings, as a kind of sandwich structures, are lightweight and mobile and thus suitable for civil, military and terrorist-protective applications. A sacrificial cladding is generally composed of a thin cover plate and a cellular core. Under a blast load, the main structure (protected structure) behind the sacrificial cladding is protected by the large deformation of the cellular core, by means of which much energy is absorbed

and the blast load is attenuated. As a result, a maximum energy absorption capacity and a minimum stress transmitted to the main structure are the two major design objectives of a cladding as a protective structure.

Shock enhancement and sequential cell collapsing are typical features of dynamic response of cellular materials under intense dynamic load, such as blast load and high-velocity impact. The shock enhancement brings the increase of energy absorption capacity and the mechanism of sequential cell collapsing achieves the reduction of transmitted stress. It is due to these features that cellular materials have significant potential application in sacrificial claddings for blast alleviation. An idea of structural shock wave was introduced by Reid and Peng [1997] to describe this dynamic response and thus a simple continuum-based shock model was proposed by using a rate-independent, rigid–perfectly plastic–locking (R-PP-L) material idealization. Only two key parameters are included in this material idealization: the plateau stress σ_p and the densification strain ε_D. A number of studies [Harrigan *et al.*, 1999; Reid and Peng, 1997; Tan *et al.*, 2005a, b] have demonstrated that the R-PP-L shock model provides much convenience in analytical derivation and a good first-order evaluation of the dynamic response of cellular materials. With using more accurate material idealizations but retaining the theoretical basis, some other shock models, were further developed in the literature [Harrigan *et al.*, 2010; Harrigan *et al.*, 2005; Lopatnikov *et al.*, 2007; Lopatnikov *et al.*, 2003; Pattofatto *et al.*, 2007; Zheng *et al.*, 2012].

However, several interesting but counterintuitive experimental observations make the protective function of cellular materials seem questionable. Cooper *et al.* [1991] reported that the transmitted stress through a foam layer is significantly enhanced, and visceral injury on animals is significantly augmented rather than alleviated when foam is used as "protective" layer. Similarly, enhancements of transmitted stress through foams are also observed in Refs. [Ben-Dor *et al.*, 1994; Skews *et al.*, 1993]. Li and Meng [2002] proposed a one-dimensional spring-mass model to qualitatively investigate these phenomena. They found a stress enhancement/attenuation boundary of loading parameters, which means that a cellular material can attenuate the blast load only when the blast load is below a critical value. Moreover, they demonstrated that the conditions for transmitted stress enhancement are almost the same as the conditions for full densification of the cellular material. Based on shock models, Harrigan *et al.* [2010] argued that transmitted stress enhancement never occurs during the propagation of the compaction wave through a cellular material and it only occurs when full densification of the cellular material occurs. Both the results in [Li and Meng, 2002] and [Harrigan *et al.*, 2010] indicate that a sacrificial cladding with a sufficiently thick cellular core can definitely serve as a protective function against blast load. Thus, in practical applications, the proper design of a sacrificial cladding is important. For the case of a sacrificial cladding under triangular pressure pulse, Hanssen *et al.* [2002] analytically obtained the minimum thickness of a cellular core required to fully

absorb the given blast load by using the R-PP-L idealization. When the thickness exceeds the minimum value, the transmitted stress through the cladding is limited to the plateau stress of the cellular core.

For a sacrificial cladding with a single-layer cellular core (namely a single-layer cellular cladding, short as SLCC hereinafter), to increase its energy absorption capacity, one should increase the thickness or the relative density of the cellular core. However, an increase of thickness is not applicable when the thickness of the cladding is stringently required, especially for a limitation of work space in some practical applications. An increase of relative density results in a high plateau stress and therefore the transmitted stress may be higher than the allowable stress of the protected structure. To overcome these limitations, Ma and Ye [2007b] suggested a double-layer foam cladding (namely a double-layer cellular cladding, short as DLCC hereinafter) comprising two layers with different density foams and considered two typical configurations, i.e. C-I: cladding with low-density foam close to the blast load and C-II: cladding with high-density foam close to the blast load. They found that the blast resistant capacity of C-II is smaller than that of C-I. On the other hand, Liao *et al.* [2012] reported that, from a design perspective, C-II is more suitable for protective structures than C-I because it has the potential in terms of large energy absorption with a low stress level transmitted to the protected structures. By using strain field calculation method, they further observed the possibility that the high-density cellular core in C-II is not fully utilized, which indicates that the blast resistant capacity of C-II can be improved through an optimal design of the thicknesses of the two cellular cores. Motivated by these observations, this paper conducts an optimal design of the layer thicknesses of a DLCC, in which the cellular core layer with high density is placed close to the blast load.

Besides the cellular core, the cover plate in a sandwich structure also influences the dynamic response of the structure under a blast load. Xue and Hutchinson [2003] found that among sandwich plates of the same total mass, the initial kinetic energy imparted to structure increases with reducing the thickness of the cover plate towards the blast. The minimum thickness of the cellular core in a SLCC required to fully absorb the blast load obtained by Hanssen *et al.* [2002] is related to the mass ratio between the cover plate and the cellular core. Compared to a SLCC, a DLCC introduces not only another cellular core, but also another plate between the cellular cores. The influence of cover plates on the dynamic response of DLCCs needs further study.

In Section 2, shock wave propagations in DLCCs with cellular cores of identical density and different densities are studied by using the one-dimensional shock model with the R-PP-L material idealization. Closed-form solution of critical thicknesses of DLCCs with cellular cores of identical density is given. In Section 3, response features of DLCCs of different densities are analyzed and then the layer thicknesses of a DLCC are optimized to determine the critical thickness. In Section 4, sacrificial claddings for blast alleviation are compared and a design method is presented,

thereafter the theoretical predictions are compared with cell-based finite element (FE) results. Finally, conclusions are summarized in Section 5.

2. Sacrificial Claddings for Blast Alleviation

For an explosion in reality, the blast load applied to a cladding is actually the pressure reflected from the cover plate of the cladding and thus it is a consequence of the interaction between the blast pressure wave produced by the explosive and the motion of the cladding. This coupling effect, i.e. fluid-structure interaction (FSI) effect, has been investigated by numerous studies [Kambouchev *et al.*, 2006; Main and Gazonas, 2008; Nian *et al.*, 2012; Vaziri and Hutchinson, 2007; Wang *et al.*, 2011]. Most recently, Nian *et al.* [2012] numerically studied the dynamic compaction of foam produced by a blast pressure wave and found that the FSI effect is significant only in the early stage of the blast pressure history. In this paper, for the purpose of simplicity the blast load is assumed to be a pressure uniformly acting on the cladding and pre-defined as a triangular pressure pulse as in [Hanssen *et al.*, 2002; Ma and Ye, 2007a, b]

$$p(t) = \begin{cases} p_0 (1 - t/t_0), & 0 \le t \le t_0 \\ 0, & t > t_0 \end{cases}, \tag{1}$$

where p_0 is the initial peak pressure and t_0 is the duration of the blast load.

Several kinds of sacrificial claddings, serving as protective function from explosive blast load, have been investigated theoretically, experimentally and numerically in the literature. For example, a SLCC is proposed by Hanssen *et al.* [2002], as illustrated in Fig. 1a. To enhance the blast resistant capacity, Ma *et al.* [2007b] suggested a DLCC made of different cellular materials, as illustrated in Fig. 1b. In theoretical analysis, the sacrificial cladding is commonly assumed to be a unit strip and investigated based on a one-dimensional stress wave theory because of the approximate one-dimensional dynamic response of the cladding. The cover plate is considered to be rigid. For the purpose of simplicity, the protected structure is usually considered to be a rigid component and then only transmitted stress to this component is needed to assess the protective function of the cladding. The R-PP-L shock model has benefits of simple derivation in theoretical analysis and probably offers closed-form solutions, which are convenient for structural design and engineering applications. Therefore, it is employed in this paper to investigate the dynamic response of cellular materials in claddings.

Based on the R-PP-L shock model, the transmitted stress to the protected structure is limited to the plateau stress of the cellular core close to the structure before it is fully compacted. From a design perspective, the optimal cellular material close to the protected structure is the material whose plateau stress σ_p equals to the allowable stress of the protected structure σ_0, i.e. $\sigma_p = \sigma_0$. If $\sigma_p < \sigma_0$, it requires a thicker cellular material to dissipate the energy so that the cladding is not economically utilized; while if $\sigma_p > \sigma_0$, the cladding loses its protective function.

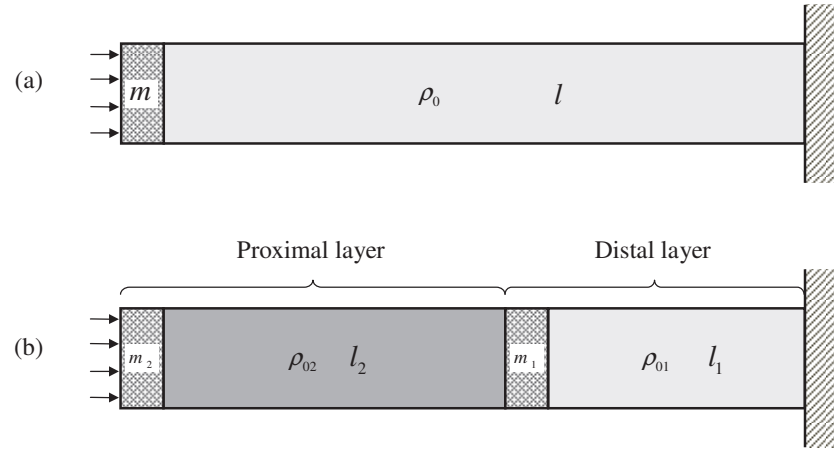

Fig. 1. Sacrificial claddings for blast alleviation: (a) a single-layer cellular cladding (SLCC); (b) a double-layer cellular cladding (DLCC).

Thus, once the protected structure is given, the plateau stress of the cellular material close to the protected structure is determined. For most of cellular materials, Gibson and Ashby [1997] reported that most properties of a cellular material, such as plateau stress σ_p and densification strain ε_D, are a function of its relative density and provided scaling relations for several cellular materials by theoretical analysis or fitting from experimental data. These scaling relations provide much convenience for design of sandwich structures with cellular materials in practical engineering applications. Therefore, once the plateau stress is determined, the cellular material can be easily specified by choosing the relative density.

For fully absorbing blast load, conservation of momentum for the whole system requires that the impulse exerted by the cellular core on the protected structure should equal the impulse exerted by the blast load, i.e. $\sigma_p t_m = p_0 t_0/2$, where t_m is the time the stress σ_p acts on the protected structure. Suppose that t_m is longer than the duration of the blast load t_0, i.e. $t_m > t_0$, it leads to $p_0 > 2\sigma_p$, which is the situation that we do consider when a sacrificial cladding serves as a protective function against blast load.

2.1. *Single-Layer Cellular Cladding (SLCC)*

Consider a strip of a SLCC of unit cross-sectional area with cellular core of initial density ρ_0, plateau stress σ_p and densification strain ε_D, as illustrated in Fig. 1a. The mass per unit area of the cover plate is m, but the thickness of the cover plate is ignored. The critical thickness of the SLCC required to fully absorb the blast load

is given by Hanssen *et al.* [2002] as

$$l_0 = \frac{m}{\rho_0}\left[-1+\sqrt{1+S\left(1-\frac{4\sigma_{\mathrm{p}}}{3p_0}\right)}\right], \quad \frac{p_0}{\sigma_{\mathrm{p}}} > 2, \tag{2}$$

where S is a dimensionless number, namely the shock-enhancement factor, defined as

$$S = \frac{\rho_0 \left(p_0 t_0/2m\right)^2}{\sigma_{\mathrm{p}}\varepsilon_{\mathrm{D}}}. \tag{3}$$

The maximum velocity that the cover plate can reach is the velocity when total blast impulse is transferred to the cover plate and the cellular core is neglected, i.e. $p_0 t_0/2m$. Thus, the shock-enhancement factor S represents the ratio between the shock enhancement of the cellular material impacted by the cover plate with its maximum velocity and the plateau stress of the cellular material.

Note that the cover plate itself can not absorb energy, but it has an influence on the energy absorption of the whole cladding, as implicated in Eq. (2). Differentiating l_0 with respect to m leads to

$$\rho_0 \frac{dl_0}{dm} = \frac{1}{\sqrt{1+S\left(1-4\sigma_{\mathrm{p}}/3p_0\right)}} - 1. \tag{4}$$

It is evident that $dl_0/dm < 0$ since $S > 0$ and $p_0/\sigma_p > 2$. This indicates that the critical thickness l_0 decreases monotonically with the increase of the mass of the cover plate m. The reason is that a larger mass subjected to blast impulse results in a smaller kinetic energy ($\sim (p_0 t_0)^2/8m$) available in the cover plate, which requires a thinner cellular material to dissipate. This effect was previously reported by Xue and Hutchinson [2003] in a numerical study of sandwich plates subjected to blast load that a thinner face sheet towards blast load results in a higher initial kinetic energy imparted to structure. In experimental study, however, the cover plate enhancing energy transfer was observed by Hanssen *et al.* [2002] in a study of SLCC under close-range blast load. Surface effects corresponding to the shape change of the cover plate is attributed to the enhancement of energy transfer. In fact, this surface effect is essentially the FSI effect. Therefore, at least two effects determine the influence of the cover plate on the dynamic response of cladding under blast load in practical applications. Besides, the cover plate has a function of protecting cellular materials from disintegrating during blast load, as observed in [Hanssen *et al.*, 2002].

From Eq. (4), it is also evident that $d(\rho_0 l_0 + m)/dm > 0$, which means that the total mass of the SLCC increases monotonically with increasing the mass of the cover plate m. Therefore, a larger mass of the cover plate results in a thinner cellular material but also a larger total mass of the cladding. Hence, the larger mass of the cover plate is not always the better in practical applications. Instead, the mass of the cover plate should be properly chosen by considering the requirement of the mass of the whole cladding. After all, one reason for using cellular material is to achieve a lightweight energy absorber.

Compared to a SLCC, a DLCC introduces not only another cellular core but also another plate. In order to merely investigate the influence of this additional plate, a DLCC with cellular cores of identical density (denoted as Cladding-1 hereinafter) is first considered, as presented in Section 2.2. The dynamic response of a DLCC with cellular cores of different densities will be investigated in Section 2.3.

2.2. *Double-layer cellular cladding with cellular cores of identical density*

Consider a unit strip of Cladding-1, as illustrated in Fig. 2. This cladding consists of two layers, i.e. the proximal layer close to blast load and the distal layer close to rigid support surface. The two layers are assumed to be bonded perfectly. The two cellular cores have the same initial density ρ_0, plateau stress σ_p and densification strain ε_D, but they may have different thicknesses, which are l_2 for the cellular core in the proximal layer and l_1 for that in the distal layer. The mass per unit area of the plates in the proximal layer and the distal layer are m_2 and m_1, respectively.

Once a blast load with $p_0 > 2\sigma_p$ is applied to Cladding-1, an elastic precursor wave travels through the cladding with infinite speed based on the rigid nature assumed by the R-PP-L idealization. The stress-strain state in the material instantaneously changes from ($\sigma = 0$, $\varepsilon = 0$) to (σ_p, 0). Following the elastic precursor wave, a plastic shock wave with finite speed initiates near the cover plate in the proximal layer and travels from the proximal layer to the distal layer. Thus,

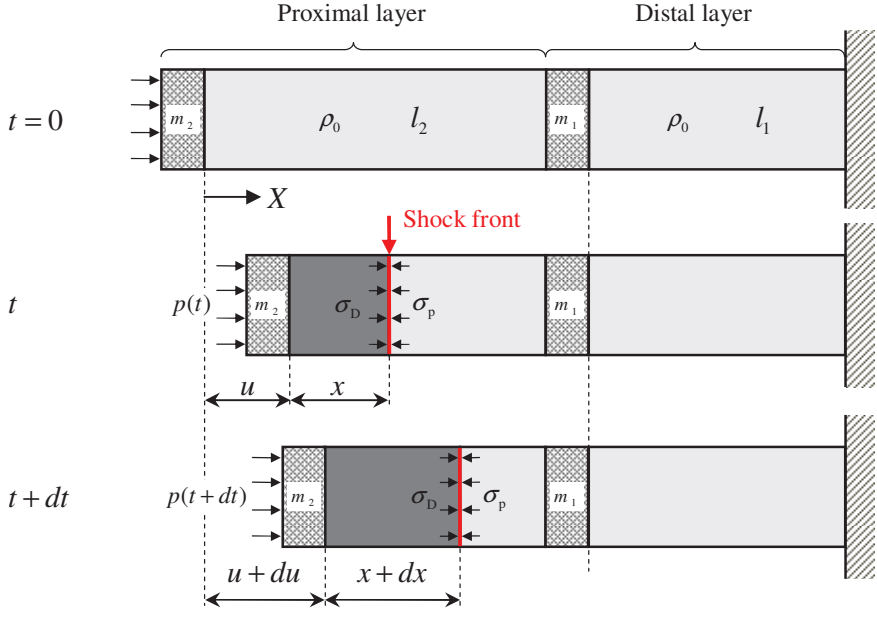

Fig. 2. Schematic representation of Cladding-1 under blast load.

Cladding-1 deforms progressively from the proximal layer to the distal layer. After the plastic shock wave passes through the material, it is compacted and the stress-strain state is further raised from (σ_p, 0) to (σ_D, ε_D), as depicted in Fig. 2. As the blast pressure reduces, an elastic unloading wave with infinite speed initiates and attenuates the plastic shock wave. The plastic shock wave can continue to propagate through the cellular core even after the end of the blast load because of the kinetic energy available in the rigid part (cover plate and compacted region of cellular material). Thereafter, the situation is equivalent to a rigid mass with initial velocity striking the cellular core as investigated in [Reid and Peng, 1997; Tan *et al.*, 2005b; Zheng *et al.*, 2012]. Similarly, the strength of the plastic shock wave is attenuated because the velocity of the rigid mass decreases due to the stress right behind the plastic shock front. Once the proximal layer is fully compacted, it collides with the cover plate of the distal layer and it can be assumed that the proximal layer will move together with the cover plate of the distal layer at the same velocity. If $p_0 \leq 2\sigma_p$, the plastic shock wave vanishes during the blast pressure history ($t < t_0$), as discussed in [Hanssen *et al.*, 2002]. If $p_0 \leq \sigma_p$, there is no plastic shock wave and the cellular cores do not deform.

As derived in Appendix A, the critical thickness of Cladding-1 required to fully absorb the blast load, l_{CR1}, is determined as

$$l_{\mathrm{CR1}} = \frac{m_1 + m_2}{\rho_0}\left[-1 + \sqrt{1 + \frac{2\rho_0 l_2}{(1+\eta)^2 m_1} + S_2\left(1 - \frac{4\sigma_{\mathrm{p}}}{3p_0}\right)}\right], \tag{5}$$

where η is the mass ratio of the plates in the proximal layer and the distal layer, i.e.

$$\eta = m_2/m_1, \tag{6}$$

and S_2 is the shock-enhancement factor, given by

$$S_2 = \frac{\rho_0 \left[p_0 t_0/2\left(m_1 + m_2\right)\right]^2}{\sigma_{\mathrm{p}}\varepsilon_{\mathrm{D}}}. \tag{7}$$

It is indicated from Eq. (5) that the critical thickness depends not only on the mass of the two cover plates but also on the thickness of the proximal layer.

Differentiating l_{CR1} with respect to m_2, m_1 and l_2 leads to

$$\rho_0 \frac{dl_{\mathrm{CR1}}}{dm_2} = \frac{1}{1 + \rho_0 l_{\mathrm{CR1}}/\left(m_1 + m_2\right)} - 1, \tag{8}$$

$$\rho_0 \frac{dl_{\mathrm{CR1}}}{dm_1} = \frac{1 + \rho_0 l_2/\left(m_1 + m_2\right)}{1 + \rho_0 l_{\mathrm{CR1}}/\left(m_1 + m_2\right)} - 1, \tag{9}$$

$$\frac{dl_{\mathrm{CR1}}}{dl_2} = \frac{1}{(1+\eta)\left[1 + \rho_0 l_{\mathrm{CR1}}/\left(m_1 + m_2\right)\right]}. \tag{10}$$

It is evident that $dl_{CR1}/dm_2 < 0$ while $dl_{CR1}/dl_2 > 0$, indicating that the critical thickness l_{CR1} decreases monotonically with increasing m_2 while increases

monotonically with increasing l_2. Note that $l_{CR1} > l_2$ except the limit case that Cladding-1 in fact is converted into a SLCC where $l_{CR1} = l_2$, indicating that $dl_{CR1}/dm_1 < 0$. Thus, the critical thickness l_{CR1} also decreases monotonically with m_1. It transpires that the cover plates in the proximal layer and the distal layer have a similar influence on the dynamic response of Cladding-1.

2.3. *Double-layer cellular cladding with cellular cores of different densities*

Consider a unit strip of a DLCC comprising cellular cores of different densities, as illustrated in Fig. 3. The initial density ρ_0, plateau stress σ_p and densification strain ε_D of the cellular core and the mass per unit area of the cover plate m are denoted with subscript 2 for the proximal layer and 1 for the distal layer. The DLCC under concern in the current study is the cladding in which the density of the cellular core in the proximal layer, ρ_{02}, is larger than that of the cellular core in the distal layer, ρ_{01}. This particular kind of DLCC is marked as Cladding-2 hereinafter.

Besides the case that $p_0 > 2\sigma_{p1}$ as previously discussed, another condition that $p_0 > \sigma_{p2}$ is also introduced to make the strong cellular material in the proximal layer experience plastic deformation for energy absorption as the cellular material in the distal layer. Once a blast load is applied to Cladding-2, an elastic precursor

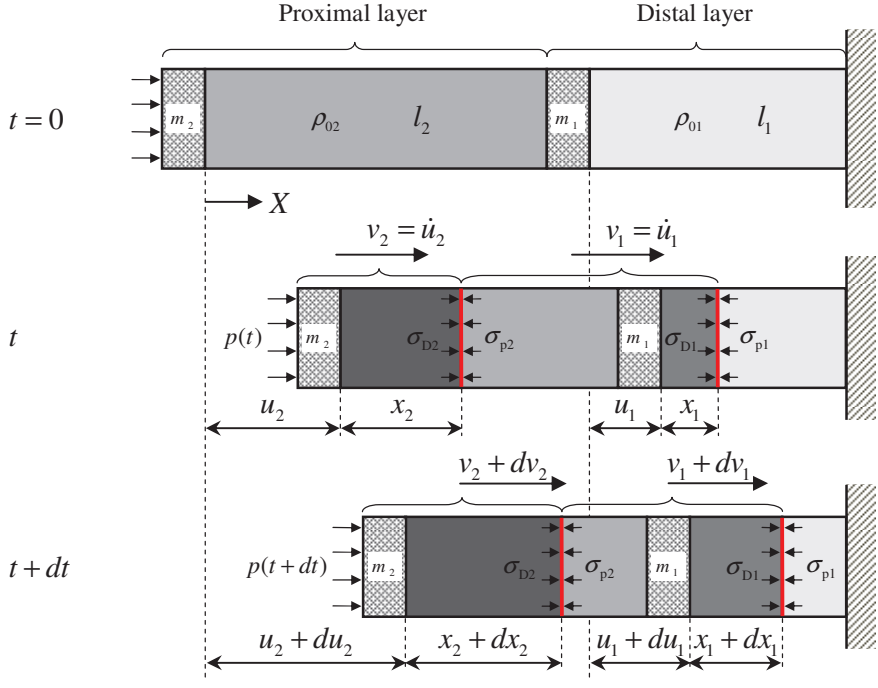

Fig. 3. Schematic representation of Cladding-2 under blast load.

wave initiates and travels through the cladding with infinite speed. The stresses in the proximal layer and the distal layer are instantaneously raised to σ_{p2} and σ_{p1}, respectively. Following the elastic precursor wave, two plastic shock waves simultaneously initiate, i.e. one in the proximal layer near the cover plate and the other in the distal layer near the cover plate, and therefore the proximal layer and the distal layer deform simultaneously. As the plastic shock waves propagate through the cellular cores, the stress-strain states in the proximal layer and the distal layer, as depicted in Fig. 3, change from $(\sigma_{p2}, 0)$ to $(\sigma_{D2}, \varepsilon_{D2})$ and from $(\sigma_{p1}, 0)$ to $(\sigma_{D1}, \varepsilon_{D1})$, respectively. Before the distal layer is fully compacted, the stress on the support surface (stress transmitted to the protected structure) is limited to σ_{p1}, which is required for Cladding-2 as a protective structure and definitely, this can be roughly achieved by choosing a sufficiently thick cellular core in the distal layer.

The governing equations of the motion of Cladding-2 described by the displacement of the cover plate in the proximal layer, u_2, and that of the cover plate in the distal layer, u_1, are derived in Appendix B as

$$\left[m_2 + \frac{\rho_{02}}{\varepsilon_{\mathrm{D2}}}\left(u_2 - u_1\right)\right]\ddot{u}_2 + \frac{\rho_{02}}{\varepsilon_{\mathrm{D2}}}\left(\dot{u}_2 - \dot{u}_1\right)^2 + \left[\sigma_{\mathrm{p2}} - p(t)\right] = 0, \tag{11}$$

and

$$\left[\rho_{02} l_2 - \frac{\rho_{02}}{\varepsilon_{\mathrm{D2}}}\left(u_2 - u_1\right) + m_1 + \frac{\rho_{01}}{\varepsilon_{\mathrm{D1}}}u_1\right]\ddot{u}_1 + \frac{\rho_{01}}{\varepsilon_{\mathrm{D1}}}\dot{u}_1^2 + \left(\sigma_{\mathrm{p1}} - \sigma_{\mathrm{p2}}\right) = 0. \tag{12}$$

Since the duration of the blast load is very short, it is assumed that the blast load has reduced to zero before the proximal layer is fully compacted. After the end of the blast load, the proximal layer continues to be crushed because of the kinetic energy available in the cover plate and the compacted region of the proximal layer. Initially, $\dot{u}_2 = \dot{u}_1 = 0$ and $p_0 > \sigma_{p2}$ at $t = 0$, it is found that the acceleration of the cover plate in the proximal layer $\ddot{u}_2 > 0$ from Eq. (11). As time increases, $p(t)$ reduces and therefore there exists a certain time after that $\ddot{u}_2 < 0$. Thus, the velocity of the cover plate in the proximal layer increases with time at the early stage. After it reaches the maximum value over a small time interval, it decreases with time. Similarly, Eq. (12) implies that the velocity of the cover plate in the distal layer also increases with time at the early stage, while it may reach a constant value at a certain time. Thus, the deformation of Cladding-2 can be divided into three successive phases:

(1) Phase I: $0 < t \leq t_0$.
The governing equations follow Eqs. (11) and (12). The initial conditions are $u_2(0) = u_1(0) = 0$ and $\dot{u}_2(0) = \dot{u}_1(0) = 0$.
(2) Phase II: $t_0 < t \leq t_1$.
Based on the above analysis, there are two possible scenarios for the deformation of Cladding-2 in Phase II. One scenario is that the proximal layer is fully compacted earlier than the distal layer and subsequently impacts the rigid part

of the distal layer (cover plate and the compacted region of the cellular core). It is assumed that the proximal layer will move together with the rigid part in the distal layer at the same velocity, which can be obtained by the conservation of momentum. The other scenario is that the velocity of the cover plate in the proximal layer decreases to be the same as that of the cover plate in the distal layer, and subsequently the proximal layer stops deforming and moves together with the cover plate in the distal layer. Hence, t_1 is the time when the proximal layer is fully compacted or the time when the velocity of the cover plate in the proximal layer decreases to be the same as that of the cover plate in the distal layer.

The governing equations in Phase II also follow Eqs. (11) and (12), while recognizing that the term of blast load in Eq. (11), $p(t)$, vanishes in this phase. The initial conditions for Phase II are the displacements and velocities of the two cover plates at the end of Phase I.

(3) Phase III: $t_1 < t \leq t_m$.

The time t_m corresponds to fully absorption of the impulse exerted by the blast load. In this phase, the deformation of Cladding-2 is equivalent to a rigid mass (the proximal layer and the compacted region of the distal layer at the end of Phase II) striking a cellular core (the uncompacted cellular core in the distal layer) with an initial velocity, whose theoretical solution can be found in [Reid and Peng, 1997; Tan *et al.*, 2005b; Zheng *et al.*, 2012]. The initial conditions for Phase III are the displacement and velocity of the cover plate in the distal layer at the end of Phase II.

With the governing equations and initial conditions, the time histories of the displacements (u_2, u_1) and the velocities (v_2, v_1) of the both cover plates can be numerically determined by employing the fourth-order Runge-Kutta scheme, since closed-form solutions can not be obtained. In the next section, the response features of Cladding-2 under blast poses a design problem by seeking the thickness distribution of the two cellular cores that minimizes the total thickness of Cladding-2 for fully absorbing blast load, resulting in the critical thickness l_{CR2}.

3. Critical Thickness of Cladding-2

3.1. *Response features*

For most of cellular materials, Gibson and Ashby [1997] reported that most properties of a cellular material are a function of its relative density. The scaling relations can be given as

$$\sigma_{\mathrm{p}}/\sigma_{\mathrm{y}} = c\,(\rho_0/\rho_{\mathrm{s}})^n\,, \tag{13}$$

and

$$\varepsilon_{\mathrm{D}} = \alpha_1 - \alpha_2\,(\rho_0/\rho_{\mathrm{s}})\,, \tag{14}$$

where ρ_s and σ_y are the density and the yield stress of the solid material, respectively; c, n, α_1 and α_2 are constant coefficients obtained by theoretical analysis or fitted by experimental data. Most recently, Wang *et al.* [2012] obtained the coefficients in Eqs. (13) and (14) by fitting from numerical data of Voronoi honeycombs (as used in this paper to model the cellular materials) as $c = 0.543$, $n = 2$, $\alpha_1 = \alpha_2 = 0.725$. The solid material of Voronoi honeycombs for the present study is assumed to be elastic, perfectly plastic with density $\rho_s = 2700\,\mathrm{kg/m^3}$, Young's modulus $E = 66\,\mathrm{GPa}$, yield stress $\sigma_y = 175\,\mathrm{MPa}$ and Poisson's ratio $\nu = 0.3$. Two honeycombs are selected to demonstrate the response features of Cladding-2. In this section, the mechanical properties of the honeycomb used in the proximal layer are $\rho_{02} = 405\,\mathrm{kg/m^3}$, $\sigma_{p2} = 2.14\,\mathrm{MPa}$, $\varepsilon_{D2} = 0.62$ and those of the honeycomb used in the distal layer are $\rho_{01} = 270\,\mathrm{kg/m^3}$, $\sigma_{p1} = 0.95\,\mathrm{MPa}$, $\varepsilon_{D1} = 0.65$. Both the cover plates have a mass per unit area $m_1 = m_2 = 2.7\,\mathrm{kg/m^2}$, which is approximately the mass per unit area of an aluminum plate with a thickness of 1 mm. The blast load is defined by initial peak pressure of $p_0 = 20\,\mathrm{MPa}$ and duration of $t_0 = 0.3\,\mathrm{ms}$. The time corresponding to fully absorption of the blast load is $t_m = p_0 t_0/(2\sigma_{p1}) = 3.16\,\mathrm{ms}$. From Eq. (2), the critical thickness of SLCC with cellular core of density ρ_{01} and cover plate of mass $m = m_1 + m_2 = 5.4\,\mathrm{kg/m^2}$ is obtained as $l_0 = 205.29\,\mathrm{mm}$.

Typical time histories of the velocities of the two cover plates (v_2 and v_1) and the position X of the shock front are shown in Figs. 4–6. In these figures, the total thicknesses of Cladding-2s are kept constant and taken to be the same as l_0, while changing the thickness ratio of the two cellular cores l_2/l_1. In Phase I, the velocity of the cover plate in the proximal layer, v_2, first increases and then decreases. This acceleration transition occurs once $p(t) = \sigma_{D2}$, and therefore v_2 starts to decrease before the blast load reduces to zero, thereafter it continues to decrease in Phase II. The velocity of the cover plate in the distal layer, v_1, however, increases in both

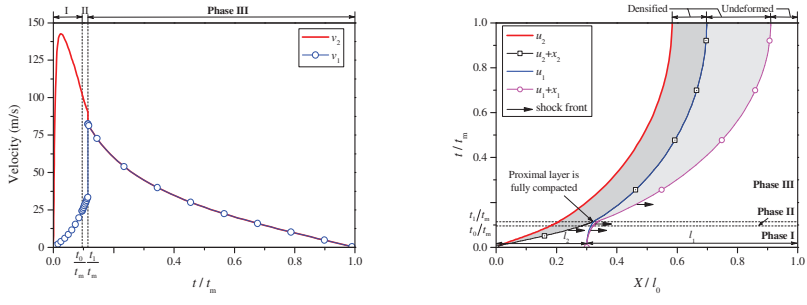

(a) (b)

Fig. 4. Time histories of (a) velocities (v_2, v_1) and (b) the position X of the shock front. $l_2/l_1 = 3/7$.

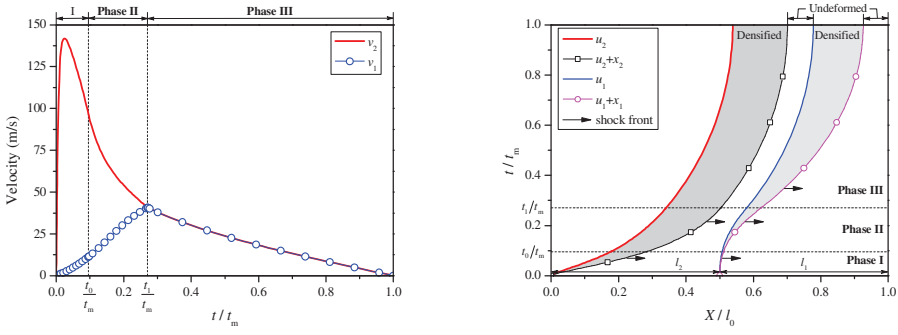

(a) (b)

Fig. 5. Time histories of (a) velocities (v_2, v_1) and (b) the position X of the shock front. $l_2/l_1 = 1$.

Phase I and Phase II. There are two shock fronts propagating through Cladding-2 in both Phases I and II, while only one shock front in Phase III.

For Cladding-2 with thin proximal layer and thick distal layer (e.g. $l_2/l_1 = 3/7$), the proximal layer becomes fully compacted before v_2 decreases to v_1, as shown in Fig. 4a. When the proximal layer impacts and bonds with the cover plate in the distal layer, there is a sudden drop of v_2 and a sharp increase of v_1, resulting in $v_2 = v_1$ at the beginning of Phase III. In this case, there is an undeformed zone in the distal layer when the blast load has been fully absorbed, as shown in Fig. 4b. It is indicated that, compared to a SLCC, thinner Cladding-2 can absorb the same blast load. As the thickness of the proximal layer increases (e.g. $l_2/l_1 = 1$), v_2 decreases to v_1 before the proximal layer is fully compacted, as shown in Fig. 5. Thereafter, the proximal layer does not deform and only the distal layer is crushed. The proximal layer and the distal layer each have an undeformed zone when the whole response

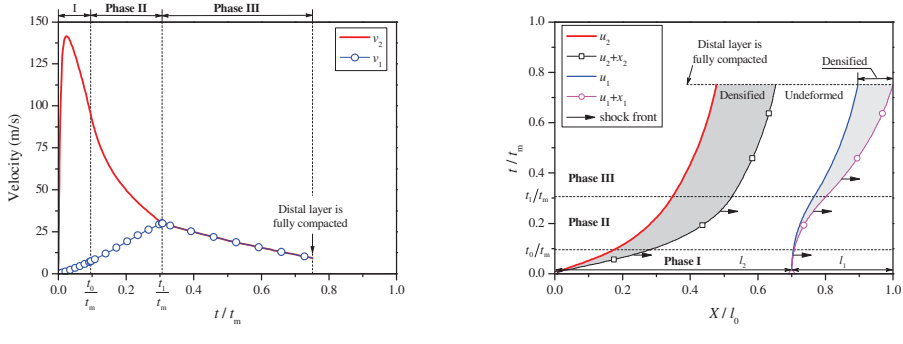

(a) (b)

Fig. 6. Time histories of (a) velocities (v_2, v_1) and (b) the position X of the shock front. $l_2/l_1 = 7/3$.

ends. For Cladding-2 with thick proximal layer and thin distal layer (e.g. $l_2/l_1 = 7/3$), v_2 also decreases to v_1 before the proximal layer is fully compacted, as shown in Fig. 6. However, the distal layer becomes fully compacted before the blast load is fully absorbed, resulting in undesired stress enhancement on the support surface. In this case, Cladding-2 loses its expected protective function, although there is still an undeformed zone in the proximal layer.

3.2. *Critical thickness*

The response features presented above demonstrate that the thickness distribution of Cladding-2 can be optimized to fully utilize the two cellular cores and obtain a minimum total thickness, namely the critical thickness. For the case of $l_2/l_1 = 3/7$, the proximal layer becomes fully compacted before v_2 decreases to v_1 so the energy absorption potential of the proximal layer has not yet been fully tapped. This is because higher density cellular material can absorb more energy per unit thickness, and therefore a proper thickness increase of the proximal layer can decrease the total thickness of the cladding. For the case of $l_2/l_1 = 1$, there is still an undeformed zone in the proximal layer after the blast load has been fully absorbed so the proximal layer has not yet been fully utilized. Similarly, a thick distal layer can not be fully utilized either as observed in the cases of $l_2/l_1 = 3/7$ and $l_2/l_1 = 1$ while a thin distal layer may result in stress enhancement on the support surface as observed in the case of $l_2/l_1 = 7/3$.

Thus, an optimal design of the thickness distribution of the two cellular cores in Cladding-2 can be achieved by introducing two constraints:

(1) Constraint I: the proximal layer becomes fully compacted exactly when v_2 decreases to v_1, by which the optimal thickness of the proximal layer l_2 is determined;
(2) Constraint II: the distal layer is fully compacted at the instant when the blast load is fully absorbed, by which the optimal thickness of the distal layer l_1 is determined.

By considering Constraints I and II, the critical thickness distribution of Cladding-2 with two cellular materials presented in Section 3.1 can be determined as $l_2 = 81.68\,\text{mm}$ and $l_1 = 101.86\,\text{mm}$. Typical time histories of the velocities (v_2, v_1) and the position X of the shock front for the optimal Cladding-2 are shown in Fig. 7. It demonstrates that when v_2 decreases to v_1 at the end of Phase II the proximal layer is just fully compacted, and when the blast load is fully absorbed the distal layer is just fully compacted. The critical thickness of Cladding-2 required to fully absorb the blast load, l_{CR2}, is about 11% smaller than that of SLCC, l_0. It is demonstrated that, for blast alleviation, a reduction of the cladding thickness can be achieved by using Cladding-2 instead of the SLCC.

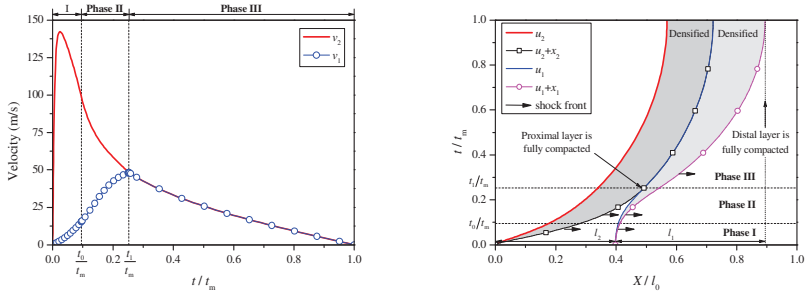

(a) (b)

Fig. 7. Time histories of (a) velocities (v_2, v_1) and (b) the position X of shock front for an optimal Cladding-2.

4. Results and Discussion

4.1. *Comparison of sacrificial claddings for blast alleviation*

Fig. 8 shows the comparison of the critical thicknesses of sacrificial claddings including a SLCC, Cladding-1 and Cladding-2. The mass of the cover plate in the SLCC, m, equals the total mass of the two cover plates in DLCCs in comparison, i.e. $m = m_1 + m_2$, which is kept constant at $m = 5.4\,\mathrm{kg/m^2}$ while changing the mass ratio η defined by Eq. (6). The density ratio ξ of cellular materials in the proximal layer and the distal layer, given by

$$\xi = \rho_{02}/\rho_{01}, \tag{15}$$

varies from 1 to 2.4, while ρ_{01} is kept constant at $270\,\mathrm{kg/m^3}$.

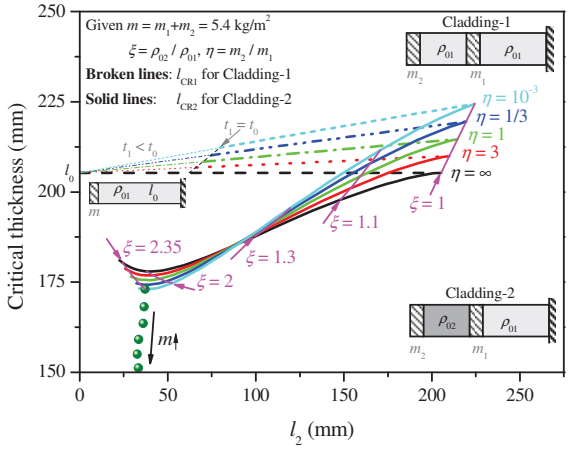

Fig. 8. Comparison of the critical thickness of sacrificial claddings.

For Cladding-1, the critical thickness, l_{CR1}, decreases with decreasing the thickness of the proximal layer l_2 or increasing the mass ratio η. When $l_2 \to 0$ or $\eta \to \infty$, corresponding to the same limit case that Cladding-1 in fact is converted into the SLCC, $l_{\mathrm{CR1}} \to l_0$. It is indicated that a SLCC is always more efficient than Cladding-1 as a protective structure for blast alleviation.

For Cladding-2, the decrease of l_2 is caused by increasing the density ratio ξ. Fig. 8 shows that the critical thickness of Cladding-2, l_{CR2}, decreases with increasing ξ until ξ increases to a certain value, then l_{CR2} starts to increase with the further increase of ξ. When ξ is small (e.g. $\xi = 1.1$), l_{CR2} decreases with increasing the mass ratio η, while it increases with increasing η when ξ is large (e.g. $\xi = 2.4$). This phenomenon reflects the interaction between two effects that influence l_{CR2}, i.e. the effect of density ratio ξ and the effect of mass ratio η. It is notable that l_{CR2} may be larger than l_0 when ξ is small, but smaller than l_0 when ξ is large enough. The relationship between l_{CR2} and ξ as well as η indicates that a maximum thickness reduction of the cladding for blast alleviation can be achieved by using Cladding-2 and choosing an optimal combination of ξ and η for each choice of the total mass of the cover plates m. For the current case in Fig. 8, the minimum critical thickness produced by $\xi = 2.35$ and $\eta = 10^{-3}$ for $m = 5.4\,\mathrm{kg/m^2}$ is $l_{\mathrm{CR2}} = 173.02\,\mathrm{mm}$, which is about 16% smaller than the critical thickness of the SLCC, $l_0 = 205.29\,\mathrm{mm}$.

As the total mass of the cover plates m in Cladding-2 increases while η is kept as 10^{-3}, the minimum l_{CR2} decreases, as shown by solid circles in Fig. 8.

4.2. *Design method for Cladding-2*

It is demonstrated that the layer thicknesses of Cladding-2 can be properly designed to fully utilize the two cellular cores, and furthermore, proper choice of the parameters in Cladding-2 can achieve a reduction of the critical thickness. For a given blast load and a protected structure, design variables of Cladding-2 are the density of the cellular core in the distal layer ρ_{01}, the total mass m and the mass ratio η of the two plates, and the density ratio ξ of the two cellular cores.

The design method for Cladding-2 against blast load is summarized as follows. Once the allowable stress of the protected structure σ_0 is given, ρ_{01} can be determined by the scaling relation Eq. (13) with the condition that $\sigma_{p1} = \sigma_0$. A larger m leads to a thinner cladding but a larger total mass of the whole cladding. Therefore, a proper choice of m should consider the requirement of the total mass of the cladding in practical applications. Once ρ_{01} and m have been determined, the only two design variables are η and ξ. By given (ξ, η), the thickness of the proximal layer l_2 is first determined from governing equations Eq. (11) and (12), scaling relations Eqs. (13) and (14) as well as Constraint I; the thickness of the distal layer l_1 is then determined by further considering Constraint II; the critical thickness of Cladding-2, $l_{\mathrm{CR2}} = l_1 + l_2$, is finally obtained. An optimal combination (ξ, η) that minimizes l_{CR2} can be sought by numerical methods, such as the conjugate gradient method.

4.3. *Comparison with cell-based FE results*

In this section, cell-based FE simulations are carried out to verify the analytical predictions about the design of Cladding-2. Both the cover plates in Cladding-2 have a mass per unit area $m_1 = m_2 = 2.7\,\mathrm{kg/m^2}$. Two Voronoi honeycombs with densities of $\rho_{02} = 540\,\mathrm{kg/m^3}$ and $\rho_{01} = 270\,\mathrm{kg/m^3}$ are used as cellular materials in the Cladding-2. In the theoretical analysis, the mechanical properties of the two honeycombs are given by Eqs. (13) and (14). The corresponding R-PP-L idealizations are shown in Fig. 9. According to Section 3.2, the optimal critical thickness distribution of the cladding can be determined as $l_2 = 45.39\,\mathrm{mm}$ and $l_1 = 130.51\,\mathrm{mm}$.

In the cell-based FE simulations, Voronoi honeycombs, generated by the 2D random Voronoi technique [Liao *et al.*, 2013; Liu *et al.*, 2009; Zheng *et al.*, 2005; Zheng *et al.*, 2013] with cell irregularity of 0.5, were employed to model the cellular materials in Cladding-2, as illustrated in Fig. 10. The specimen of Voronoi honeycomb used in the proximal layer was constructed in an area of $45.39\,\mathrm{mm} \times 50\,\mathrm{mm}$ with 575 nuclei, while that used in the distal layer was constructed in an area of $130.51\,\mathrm{mm} \times 50\,\mathrm{mm}$ with 1625 nuclei. The length of specimens in the out-of-plane direction was 1 mm. Therefore the two cover plates have a mass $M_1 = M_2 = 0.135\,\mathrm{g}$. The quasi-static nominal stress-strain curves of the two Voronoi honeycombs are shown in Fig. 9. ABAQUS/Explicit code was used to perform the

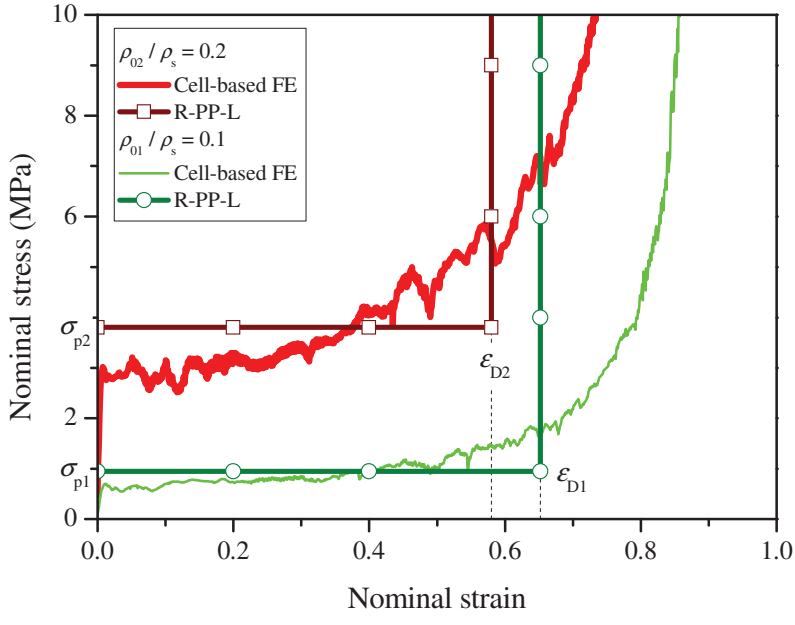

Fig. 9. Quasi-static nominal stress-strain curves of two Voronoi honeycomb specimens and their R-PP-L idealizations.

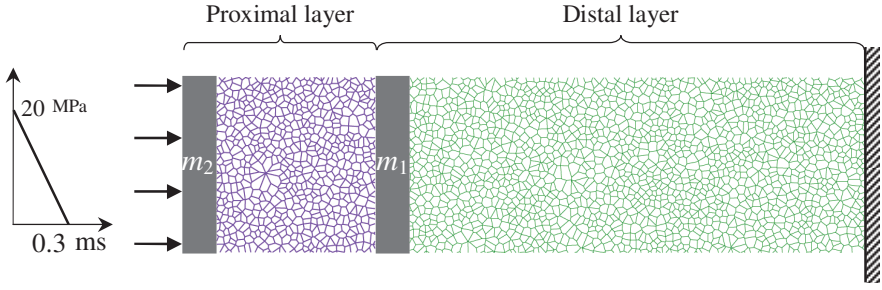

Fig. 10. Schematic representation of a Cladding-2 under blast load in the cell-based FE simulations.

FE simulations. Cell walls of specimens were modeled with S4R shell elements, of which the average length was set to be about 0.19 mm through a mesh sensitivity analysis. General contact was defined with slight friction coefficient as used in [Zheng *et al.*, 2005]. To simulate an in-plane strain state, all the nodes were constrained in the out-of-plane direction.

Comparison of the velocities of the two cover plates (v_2 and v_1) between the cell-based FE results and the analytical predictions are shown in Fig. 11a. The comparison is generally good. The cell-based FE results clearly demonstrate that the proximal layer and the distal layer almost deform simultaneously once Cladding-2 is applied to the blast load, and when the velocity of the proximal layer decreases to that of the distal layer, the two layers move together.

Time histories of the stress on the support surface in the cell-based FE results show that the distal layer is fully compacted before the blast load is fully absorbed, resulting stress enhancement on the support surface, as shown in Fig. 11b. It is notable that 92% of the total energy transferred to the Cladding-2 by the blast load has been dissipated by the cladding when the distal layer initially becomes fully compacted. The occurrence of stress enhancement implies that the thickness

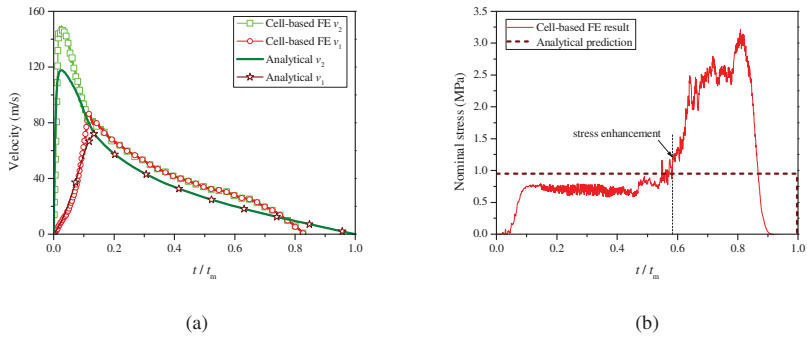

Fig. 11. Comparisons between cell-based FE results and analytical predictions: (a) velocities (v_2 and v_1); (b) stress on the support surface.

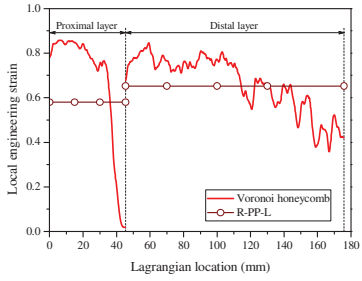

Fig. 12. Local strain distributions along the loading direction of the Voronoi honeycombs when the distal layer initially becomes fully compacted.

of the Cladding-2 is under-predicted by the theoretical analysis. This is mainly caused by the simple material model used in the theoretical analysis. The R-PP-L idealization, as shown in Fig. 9, assumes an constant densification strain so that it can not account for the nonlinear post-locking behavior of the cellular materials, which tends to over-predict the energy absorption as discussed in [Zou *et al.*, 2009]. When the distal layer initially becomes fully compacted, the local engineering strain along the loading direction of the Voronoi honeycombs, obtained by using strain field calculation method [Liao *et al.*, 2012], are shown in Fig. 12. At the early stage of the response, the velocity of the cover plate in the proximal layer, v_2 shown in Fig. 11a, is high. The high velocity results in large strain behind the shock front which is greater than the densification strain predicted by the R-PP-L shock model, as clearly demonstrated by the strain distribution in the proximal layer in Fig. 12. As the velocities of the two plates reduce, the strains in the two Voronoi honeycombs decrease. The velocity-dependence behavior of the strain is not reflected in the R-PP-L shock model. Additionally, Figs. 4–7 and 11 show that the impact velocities suffered by the cellular cores increase from zero to a higher value in Phase I and decrease with time in Phase III. At a low impact velocity, cellular materials deform in the Homogeneous Mode, in which deformation bands are randomly distributed, so the shock models are not suitable for this case. However, for simplicity, the shock models are still used in this paper. This may also be a reason for the differences between the analytical predictions and cell-based finite element results.

Despite the limitations of the R-PP-L cellular material model, the design method presented in this study gives a good guidance to the design of Cladding-2 for blast alleviation. The shock models based on more accurate material models, which account for non-linear hardening plastic behavior as discussed in [Zheng *et al.*, 2013], are expected to give a further modification to the current analytical predictions. Moreover, some graded cellular materials with continuous strength distributions may further improve the blast alleviation and energy absorption capability of sacrificial claddings. This is an interesting field worthy of future study.

5. Conclusions

A double-layer cellular cladding (DLCC) has recently been suggested to overcome the limitation of a single-layer cellular cladding (SLCC) and enhance the protective function against blast load. However, the design method for DLCCs in the literature is still not clear. In the present paper, a method for the design of a DLCC for blast alleviation is presented. Two configurations of the DLCCs are considered, i.e. cladding with cellular cores of identical density (Cladding-1) and cladding with the higher density cellular core layer close to the blast load (Cladding-2). Shock wave propagations in the two DLCCs are investigated by using the one-dimensional R-PP-L shock model. Single shock front propagates in Cladding-1, while double shock fronts propagate in Cladding-2. A closed-form expression of the critical thickness corresponding to fully absorption of blast load is derived for Cladding-1. Response features of Cladding-2 are analyzed according to different thickness ratio of the two cellular cores. Then, the layer thicknesses of the Cladding-2 are optimized to fully utilize the two cellular cores and the critical layer thicknesses of Cladding-2 can be determined.

With equal mass of the cover plates, Cladding-1 and Cladding-2 are compared with a SLCC in terms of the critical thickness. It is demonstrated that the critical thickness of Cladding-1 varies monotonically with the thickness of the proximal layer as well as the mass ratio of the two cover plates. A SLCC is always more efficient than Cladding-1 as a protective structure for blast alleviation, while Cladding-2 can be more efficient than the SLCC. Moreover, a maximum reduction of the critical thickness of Cladding-2 can be achieved by choosing an optimal combination of the density ratio of the two cellular cores and the mass ratio of the two cover plates. Then, a design method for Cladding-2 against blast load is presented. The analytical predictions of Cladding-2 are compared with the cell-based FE results in terms of the velocities of the two cover plates. Generally good agreement is observed. Some differences are observed in the comparison and analyzed through the strain distribution of Cladding-2 obtained by strain field calculation method. They are mainly caused by the simple material model used in the theoretical analysis. However, the design method presented in this study provides a simple guideline in the design of Cladding-2 for blast alleviation.

Acknowledgments

This work is supported by the National Natural Science Foundation of China (Projects Nos. 90916026 and 11002140), the Fundamental Research Funds for the Central Universities (No. WK2090050023) and the Chinese Academy of Sciences (Grant No. KJCX2-EW-L03).

Appendix A. Critical thickness of Cladding-1

The shock wave propagation in Cladding-1 under blast load is described in Section 2.2. The deformation process of Cladding-1 is illustrated in Fig. 2. Before the plastic shock wave reaches the cover plate of the distal layer, the deformation behavior of Cladding-1 is similar to that of a SLCC under blast load, which has been described by an analytical solution presented by Hanssen *et al.* [2002]. From their analysis, the displacement of the cover plate in the proximal layer is obtained as

$$u(t) = -\frac{m_2\varepsilon_{\mathrm{D}}}{\rho_0} + \varepsilon_{\mathrm{D}}\sqrt{\left(\frac{m_2}{\rho_0}\right)^2 + \frac{p_0 t_0^2}{\rho_0\varepsilon_{\mathrm{D}}}\left[-\frac{1}{3} + \frac{t}{t_0} - \left(\frac{t}{t_0}\right)^2\right]}, \tag{A.1}$$

when $t_0 < t < t_m$ and $p_0 > 2\sigma_p$. Provided that the blast load has reduced to zero before the proximal layer is fully compacted, the plastic shock wave will reach the cover plate of the distal layer at time

$$t_1 = \frac{p_0 t_0}{2\sigma_{\mathrm{p}}} - \sqrt{\left(\frac{p_0 t_0}{2\sigma_{\mathrm{p}}}\right)^2 - \frac{p_0 t_0^2 + 6m_2 l_2\varepsilon_{\mathrm{D}} + 3l_2^2\varepsilon_{\mathrm{D}}\rho_0}{3\sigma_{\mathrm{p}}}}, \tag{A.2}$$

which is derived from $u(t_1) = l_2\varepsilon_D$ since the proximal layer is fully compacted at this time. The velocity of the proximal layer at time t_1, V_1, can be obtained by differentiating Eq. (A.1) with respect to time and considering Eq. (A.2),

$$V_1 = \frac{\sqrt{9p_0^2t_0^2 - 12\left(p_0t_0^2 + 6m_2l_2\varepsilon_{\mathrm{D}} + 3l_2^2\varepsilon_{\mathrm{D}}\rho_0\right)\sigma_{\mathrm{p}}}}{6\left(m_2 + \rho_0 l_2\right)}. \tag{A.3}$$

Once the proximal layer is fully compacted, it collides with the cover plate of the distal layer with V_1. It is assumed that the proximal layer will move together with the cover plate of the distal layer at the same velocity V_2. Conservation of momentum of the system gives

$$\left(m_1 + m_2 + \rho_0 l_2\right)V_2 = \left(m_2 + \rho_0 l_2\right)V_1. \tag{A.4}$$

Thereafter, the distal layer is crushed by the rigid part (proximal layer and cover plate of the distal layer) with initial velocity V_2. If the cellular core in the distal layer is thick enough, the plastic shock wave will eventually vanish before it reaches the support surface and the blast load is fully absorbed by the crushing of the cellular cores. Otherwise, the plastic shock wave will travel the full thickness of the cladding and reflect at the support surface, resulting in a stress enhancement on the support surface, which is undesired when the cladding is used as a protective structure. According to Eq. (13) in [Harrigan *et al.*, 2010], the critical thickness of the cellular core in the distal layer to bring a mass $m_1 + m_2 + \rho_0 l_2$ with initial

velocity V_2 to rest is

$$l_{\mathrm{C}} = \left(l_2 + \frac{m_1 + m_2}{\rho_0}\right)\left(\sqrt{1 + \frac{\rho_0 V_2^2}{\sigma_{\mathrm{p}}\varepsilon_{\mathrm{D}}}} - 1\right). \tag{A.5}$$

Thus, the critical thickness of Cladding-1 required to fully absorb the blast load, $l_{\mathrm{CR1}} = l_2 + l_C$, can be obtained from Eqs. (A.3), (A.4) and (A.5) as

$$l_{\mathrm{CR1}} = -\frac{m_1 + m_2}{\rho_0} + \sqrt{\left(\frac{m_1 + m_2}{\rho_0}\right)^2 + \frac{2m_1 l_2}{\rho_0} + \frac{p_0 t_0^2}{4\rho_0\varepsilon_{\mathrm{D}}}\left(\frac{p_0}{\sigma_{\mathrm{p}}} - \frac{4}{3}\right)}, \tag{A.6}$$

which is in another form in Eq. (5).

It is notable that the critical thickness of the cladding l_{CR1} relates to the thickness of the cellular core in the proximal layer l_2. Consider two limit cases:

(1) Limit case 1: the thickness of the cellular core in the distal layer equals zero, i.e. $l_C = 0$, we have $l_2 = l_{\mathrm{CR1}}$. Substituting this condition into Eq. (A.6) leads to

$$l_{\mathrm{CR1}} = -\frac{m_2}{\rho_0} + \sqrt{\left(\frac{m_2}{\rho_0}\right)^2 + \frac{p_0 t_0^2}{4\rho_0\varepsilon_{\mathrm{D}}}\left(\frac{p_0}{\sigma_{\mathrm{p}}} - \frac{4}{3}\right)}. \tag{A.7}$$

Comparison between Eqs. (A.7) and (2) indicates that in this case Cladding-1 is converted into a SLCC with the cover plate of mass m_2 and the cellular core of density ρ_0.

(2) Limit case 2: the thickness of the cellular core in the proximal layer equals zero, i.e. $l_2 = 0$, Eq. (A.6) leads to

$$l_{\mathrm{CR1}} = -\frac{m_1 + m_2}{\rho_0} + \sqrt{\left(\frac{m_1 + m_2}{\rho_0}\right)^2 + \frac{p_0 t_0^2}{4\rho_0\varepsilon_{\mathrm{D}}}\left(\frac{p_0}{\sigma_{\mathrm{p}}} - \frac{4}{3}\right)}, \tag{A.8}$$

which is exactly the critical thickness of a SLCC with the cover plate of mass $m_1 + m_2$ and the cellular core of density ρ_0.

Appendix B. Governing Equations of Cladding-2 Under Blast Load

The deformation of Cladding-2 can be measured by the displacement of the cover plate in the proximal layer, u_2, and that of the cover plate in the distal layer, u_1, as illustrated in Fig. 3. The velocities of the cover plates in the proximal layer and the distal layer are denoted as v_2 and v_1, respectively. Conservation of mass for the cellular cores at time t relates the displacements of the cover plates, u_2 and u_1, with the compacted thicknesses of the cellular cores, x_2 and x_1, as

$$u_2 - u_1 = \frac{\varepsilon_{\mathrm{D2}}}{1 - \varepsilon_{\mathrm{D2}}} x_2, \tag{B.1}$$

$$u_1 = \frac{\varepsilon_{\mathrm{D1}}}{1 - \varepsilon_{\mathrm{D1}}} x_1. \tag{B.2}$$

Over a small time interval from t to $t+dt$, the plastic shock wave travels along the proximal layer so that a small element of material is compacted and the compacted

thickness of the cellular core increases from x_2 to $x_2 + dx_2$. The stress on the left side of the small element is raised from σ_{p2} to σ_{D2} and the velocity of the element changes from $\dot{u}_1$ to $\dot{u}_2 + d\dot{u}_2$, where superposed dots denote differentiation with respect to time. Similarly, the compacted thickness of the cellular core in the distal layer increases from x_1 to $x_1 + dx_1$. The stress on the left side of the small element in the distal layer is raised from σ_{p1} to σ_{D1} and the velocity of the element changes from 0 to $\dot{u}_1 + d\dot{u}_1$. Conservation of momentum for the two small elements in the proximal layer and the distal layer over the small time interval dt gives

$$\rho_{02}\frac{dx_2}{1-\varepsilon_{\mathrm{D2}}}\left(\dot{u}_2 + d\dot{u}_2 - \dot{u}_1\right) = \left(\sigma_{\mathrm{D2}} - \sigma_{\mathrm{p2}}\right)dt, \tag{B.3}$$

$$\rho_{01}\frac{dx_1}{1-\varepsilon_{\mathrm{D1}}}\left(\dot{u}_1 + d\dot{u}_1\right) = \left(\sigma_{\mathrm{D1}} - \sigma_{\mathrm{p1}}\right)dt. \tag{B.4}$$

In the same manner, consider two rigid parts, i.e. one consists of the cover plate and the compacted region in the proximal layer at time t and the other consists of the undeformed region in the proximal layer at time $t + dt$, the cover plate and the compacted region in the distal layer at time t. Conservation of momentum for the two rigid parts over dt gives

$$\left(m_2 + \rho_{02}\frac{x_2}{1-\varepsilon_{\mathrm{D2}}}\right)d\dot{u}_2 = \left[p(t+dt) - \sigma_{\mathrm{D2}}\right]dt, \tag{B.5}$$

$$\left(\rho_{02}l_2 - \rho_{02}\frac{x_2 + dx_2}{1-\varepsilon_{\mathrm{D2}}} + m_1 + \rho_{01}\frac{x_1}{1-\varepsilon_{\mathrm{D1}}}\right)d\dot{u}_1 = \left(\sigma_{\mathrm{p2}} - \sigma_{\mathrm{D1}}\right)dt. \tag{B.6}$$

Substituting Eqs. (B.1) and (B.3) into Eq. (B.5), neglecting the higher order terms, dividing by dt and taking the limit $dt \to 0$ leads to

$$\left[m_2 + \frac{\rho_{02}}{\varepsilon_{\mathrm{D2}}}\left(u_2 - u_1\right)\right]\ddot{u}_2 + \frac{\rho_{02}}{\varepsilon_{\mathrm{D2}}}\left(\dot{u}_2 - \dot{u}_1\right)^2 + \left[\sigma_{\mathrm{p2}} - p(t)\right] = 0. \tag{B.7}$$

Substituting Eqs. (B.1), (B.2) and (B.4) into Eq. (B.6), neglecting the higher order terms, dividing by dt and taking the limit $dt \to 0$ leads to

$$\left[\rho_{02}l_2 - \frac{\rho_{02}}{\varepsilon_{\mathrm{D2}}}\left(u_2 - u_1\right) + m_1 + \frac{\rho_{01}}{\varepsilon_{\mathrm{D1}}}u_1\right]\ddot{u}_1 + \frac{\rho_{01}}{\varepsilon_{\mathrm{D1}}}\dot{u}_1^2 + \left(\sigma_{\mathrm{p1}} - \sigma_{\mathrm{p2}}\right) = 0. \tag{B.8}$$

Eqs. (B.7) and (B.8) are the governing equations of the motion of Cladding-2 under blast load, as given in Eqs. (11) and (12).

References

Ben-Dor, G., Mazor, G., Igra, O., Sorek, S., Onodera, H. [1994] "Shock wave interaction with cellular materials. Part II: open cell foams; experimental and numerical results." *Shock Waves* **3**, 167–179.

Cooper, G. J., Townend, D. J., Cater, S. R., Pearce, B. P. [1991] "The role of stress waves in thoracic visceral injury from blast loading: Modification of stress transmission by foams and high-density materials." *J Biomech* **24**, 273–285.

Gibson, L. J., Ashby, M. F. [1997] Cellular solids: structure and properties, 2nd ed. Cambridge University Press, Cambridge, UK.

Guruprasad, S., Mukherjee, A. [2000a] "Layered sacrificial claddings under blast loading Part I – analytical studies." *Int J Impact Eng* **24**, 957–973.

Guruprasad, S., Mukherjee, A. [2000b] "Layered sacrificial claddings under blast loading Part II – experimental studies." *Int J Impact Eng* **24**, 975–984.

Hanssen, A. G., Enstock, L., Langseth, M. [2002] "Close-range blast loading of aluminium foam panels." *Int J Impact Eng* **27**, 593–618.

Harrigan, J. J., Reid, S. R., Peng, C. [1999] "Inertia effects in impact energy absorbing materials and structures." *Int J Impact Eng* **22**, 955–979.

Harrigan, J. J., Reid, S. R., Seyed Yaghoubi, A. [2010] "The correct analysis of shocks in a cellular material." *Int J Impact Eng* **37**, 918–927.

Harrigan, J. J., Reid, S. R., Tan, P. J., Yella Reddy, T. [2005] "High rate crushing of wood along the grain." *Int J Mech Sci* **47**, 521–544.

Kambouchev, N., Noels, L., Radovitzky, R. [2006] "Nonlinear compressibility effects in fluid-structure interaction and their implications on the air-blast loading of structures." *J Appl Phys* **100**, 063519.

Karagiozova, D., Langdon, G. S., Nurick, G. N. [2010] "Blast attenuation in Cymat foam core sacrificial claddings." *Int J Mech Sci* **52**, 758–776.

Li, Q. M., Meng, H. [2002] "Attenuation or enhancement—a one-dimensional analysis on shock transmission in the solid phase of a cellular material." *Int J Impact Eng* **27**, 1049–1065.

Liao, S. F., Zheng, Z. J., Yu, J. L. [2012] "On the local nature of the strain field calculation method for measuring heterogeneous deformation of cellular materials." Int J Solids Struct under review (Submitted on December 3, 2012).

Liao, S. F., Zheng, Z. J., Yu, J. L. [2013] "Dynamic crushing of 2D cellular structures: Local strain field and shock wave velocity." *Int J Impact Eng* **57**, 7–16.

Lim, Y. W., Choi, H.-J., Idapalapati, S. [2013] "Design of Alporas aluminum alloy foam cored hybrid sandwich plates using Kriging optimization." *Compos Struct* **96**, 17–28.

Liu, Y. D., Yu, J. L., Zheng, Z. J., Li, J. R. [2009] "A numerical study on the rate sensitivity of cellular metals." *Int J Solids Struct* **46**, 3988–3998.

Lopatnikov, S. L., Gama, B. A., Gillespie, J. J. W. [2007] "Modeling the progressive collapse behavior of metal foams." *Int J Impact Eng* **34**, 587–595.

Lopatnikov, S. L., Gamaa, B. A., Jahirul Haque, M., Krauthauser, C., Gillespie Jr, J. W., Guden, M., Hall, I. W. [2003] "Dynamics of metal foam deformation during Taylor cylinder – Hopkinson bar impact experiment." *Compos Struct* **61**, 61–71.

Ma, G. W., Ye, Z. Q. [2007a] "Analysis of foam claddings for blast alleviation." *Int J Impact Eng* **34**, 60–70.

Ma, G. W., Ye, Z. Q. [2007b] "Energy absorption of double-layer foam cladding for blast alleviation." *Int J Impact Eng* **34**, 329–347.

Main, J. A., Gazonas, G. A. [2008] "Uniaxial crushing of sandwich plates under air blast: Influence of mass distribution." *Int J Solids Struct* **45**, 2297–2321.

Nian, W. M., Subramaniam, K. V. L., Andreopoulos, Y. [2012] "Dynamic compaction of foam under blast loading considering fluid-structure interaction effects." *Int J Impact Eng* **50**, 29–39.

Nurick, G. N., Langdon, G. S., Chi, Y., Jacob, N. [2009] "Behaviour of sandwich panels subjected to intense air blast – Part 1: Experiments." *Compos Struct* **91**, 433–441.

Pattofatto, S., Elnasri, I., Zhao, H., Tsitsiris, H., Hild, F., Girard, Y. [2007] "Shock enhancement of cellular structures under impact loading: Part II analysis." *J Mech Phys Solids* **55**, 2672–2686.

Reid, S. R., Peng, C. [1997] "Dynamic uniaxial crushing of wood." *Int J Impact Eng* **19**, 531–570.

Skews, B. W., Atkins, M. D., Seitz, M. W. [1993] "The role of stress waves in thoracic visceral injury from blast loading: Modification of stress transmission by foams and high-density materials." *J Fluid Mech* **253**, 245–265.

Tan, P. J., Reid, S. R., Harrigan, J. J., Zou, Z., Li, S. [2005a] "Dynamic compressive strength properties of aluminium foams. Part I - experimental data and observations." *J Mech Phys Solids* **53**, 2174–2205.

Tan, P. J., Reid, S. R., Harrigan, J. J., Zou, Z., Li, S. [2005b] "Dynamic compressive strength properties of aluminium foams. Part II - 'shock' theory and comparison with experimental data and numerical models." *J Mech Phys Solids* **53**, 2206–2230.

Theobald, M. D., Langdon, G. S., Nurick, G. N., Pillay, S., Heyns, A., Merrett, R. P. [2010] "Large inelastic response of unbonded metallic foam and honeycomb core sandwich panels to blast loading." *Compos Struct* **92**, 2465–2475.

Vaziri, A., Hutchinson, J. W. [2007] "Metal sandwich plates subject to intense air shocks." *Int J Solids Struct* **44**, 2021–2035.

Wang, E. H., Wright, J., Shukla, A. [2011] "Analytical and experimental study on the fluid structure interaction during air blast loading." *J Appl Phys* **110**, 114901.

Wang, X. K., Zheng, Z. J., Yu, J. L., Wang, C. F. [2012] "Dynamic crushing models for density-graded cellular structures under high-velocity compression." Int J Mech Sci under review (Submitted on October 25, 2012).

Xue, Z. Y., Hutchinson, J. W. [2003] "Preliminary assessment of sandwich plates subject to blast loads." *Int J Mech Sci* **45**, 687–705.

Zheng, Z. J., Liu, Y. D., Yu, J. L., Reid, S. R. [2012] "Dynamic crushing of cellular materials: Continuum-based wave models for the transitional and shock modes." *Int J Impact Eng* **42**, 66–79.

Zheng, Z. J., Yu, J. L., Li, J. R. [2005] "Dynamic crushing of 2D cellular structures: A finite element study." *Int J Impact Eng* **32**, 650–664.

Zheng, Z. J., Yu, J. L., Wang, C. F., Liao, S. F., Liu, Y. D. [2013] "Dynamic crushing of cellular materials: A unified framework of plastic shock wave models." *Int J Impact Eng* **53**, 29–43.

Zou, Z., Reid, S. R., Tan, P. J., Li, S., Harrigan, J. J. [2009] "Dynamic crushing of honeycombs and features of shock fronts." *Int J Impact Eng* **36**, 165–176.